# First Astronomical Application of a Cryogenic TES Spectrophotometer

R.W. Romani, A.J. Miller, B. Cabrera, E. Figueroa-Feliciano
*Dept. of Physics, Stanford University, Stanford CA 94305-4060*

and S.W. Nam
*NIST, Boulder, CO 80303*

## ABSTRACT

We report on the first astronomical observations with a photon counting pixel detector that provides arrival time- ($\delta t = 100$ns) and energy- ($\delta E_\gamma \leq 0.15\,$eV) resolved measurements from the near IR through the near UV. Our test observations were performed by coupling this Transition Edge Sensor (TES) device to a 0.6m telescope; we have obtained the first simultaneous optical near-IR phase-resolved spectra of the Crab pulsar. A varying infrared turnover gives evidence of self-absorption in the pulsar plasma. The potential of such detectors in imaging arrays from a space platform are briefly described.

## 1. Introduction and Experimental Apparatus

There is growing interest in using cryogenic bolometer technology in array detectors that can provide imaging spectrophotometry with high quantum efficiency in the optical range. In particular, there are well established programs developing Superconducting Tunnel Junction (STJ) devices (*eg.* Peacock, *et al.* 1996) for such arrays. Manufacture and control of STJs have proved particularly challenging, but the wide range of potential applications (*eg.* Jakobsen 1999), has motivated substantial investment in this technology. We have recently demonstrated a second bolometric device for time- and energy- resolved photon detection spanning the near IR through UV (Cabrera, *et al.* 1998). This Transition-Edge Sensor(TES) device, based on the sharp superconducting-normal transition in tungsten (W) thin-films offers remarkable new capabilities for problems requiring low energy resolution time-resolved spectrophotometry at low light levels. We have tested this instrument by coupling to small telescopes at our suburban campus site. Initial test observations, including first measurements (12/98) of the Crab pulsar were reported in Romani, *et al.* (1998); here we describe in more detail our test system and new optical/IR phase-resolved pulsar spectra. Very recently, the ESA STJ group has also detected the Crab pulsar in the optical using a focal plane STJ array at the 4.2m WHT (Perryman, *et al.* 1999), albeit with lower statistics and energy resolution than achieved here.

In the present application, our detectors are 18 micron squares of 40 nm thick tungsten (W) patterned on silicon. The Si substrate is cooled below the $T_C \approx 80\,$mK transition in a Kelvin Ox 15 dilution refrigerator. By resistively heating (Joule power $\propto V^2/R$) the pixels at a fixed voltage, the W is stably driven into the transition range; a photon is detected as a temporary deficit in the required Joule power to keep the pixel at the stable set point. This 'electro-thermal' feedback speeds up recovery to the quiescent power level (Irwin 1995). Pixels with time constants as short as $2\,\mu$s have been produced, allowing photons to be counted at rates of $\sim 30\,$kHz per channel with minimal pile-up. The current deficit pulse associated with arrival of a photon is amplified via a DC SQUID array (Welty & Martinis 1993), digitized, assigned a peak height, time-stamped using a GPS receiver and recorded to computer disk.

Tungsten is grey and photons hitting the pixel are absorbed with an efficiency varying from $\gtrsim 50\%$ in the optical/UV to $\sim 10\%$ in the near IR (Palik 1985). This substantial intrinsic efficiency can, in principle, be increased to near unity by 'blackening' the surface with a passive absorber, *e.g.*, Au-black (Harris 1956). Calibration photons were introduced into the refrigerator dewar via optical fiber – we have demonstrated single photon detection from 0.3 eV ($4\,\mu$m) to the fiber cut-off at $\sim$3.5 eV ($0.35\,\mu$m); the intrinsic device sensitivity continues to the saturation energy of 10-15 eV. Such an ultra-broad band is accessible only from space where these superconducting devices offer unprecedented new sensitivity for a number of important astronomical observations. We have initiated a series of ground-based experiments to illustrate the potential of these instruments.

The substantial IR sensitivity of the detector, coupled with rapid increase in the atmosphere and telescope thermal emissivity in the near IR means that careful filtering to exclude $E_\gamma < 0.7\,$eV ($\lambda > 1.7\,\mu$m) photons was required to avoid detector saturation. Since conventional filter glasses typically absorb beyond $\sim 2.5\ \mu$m and bandpass filters transmit in discrete octaves, we have adopted a novel filtering scheme to demonstrate the sensitivity to a larger energy range than that of CCDs or conventional IR detectors. As radiation is coupled via optical fiber, we have

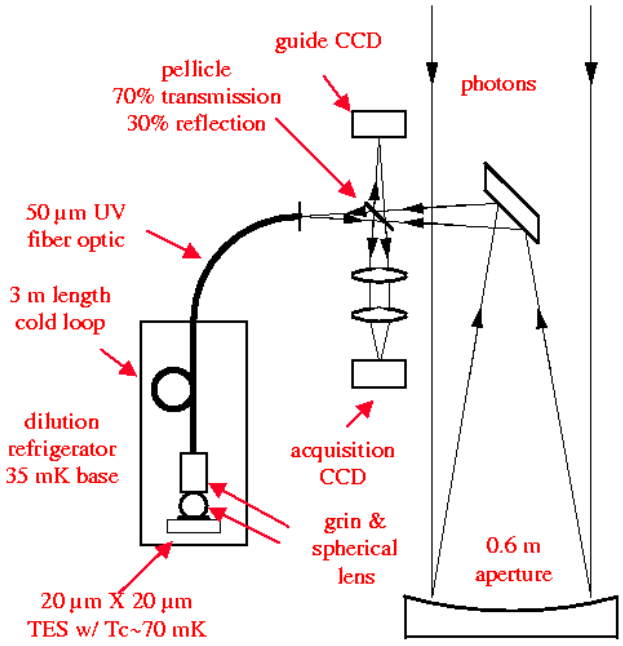


Fig. 1.— Schematic of our TES fiber coupled system at the Stanford Observatory 0.6m.

spooled 3 m of 'wet' (high OH) fiber at the 1 K stage. The OH in this fiber provides strong attenuation (Humbach 1996) below 0.7 eV and in secondary bands (e.g. 0.91 eV) where, in any case, atmospheric OH limits transmission of astrophysical signals. The system was thus sensitive from the near-IR J and H bands through the visible. Using a 50 $\mu$m core fiber we have coupled TES sensors to a 0.6 m telescope at our University teaching observatory (Fig 1). The fiber, whose core subtended 4.8″ at the f/3.5 Newtonian focus, was mounted in a reflective decker and was viewed through a pellicle by an acquisition camera. At the cold stage, the fiber output was focused through a ball and GRIN lens system to improve matching to isolated 18 $\mu$m square pixels. As focusing was incomplete, ∼25% of the photons fell on the (unmasked) voltage bias leads of the pixels (Cabrera, *et al.* 1998), for which incomplete energy transfer to the W produced pulses with $\leq 0.5$ of the main photon energy. The contribution of these 'rail hits' to the energy PSF appears in the monochromatic calibration photon spectrum in Figure 4. Photon pulses were digitized with 6 bit resolution, time-stamped to 0.1 $\mu$s precision and recorded for later analysis.

Observations of the faint visible/IR spectrophotometric standards HD 73616 and HD 284504 (Gunn and Stryker 1983) allowed an estimate of the system efficiency. The atmosphere and fiber plus detector system showed ∼ 2% peak effective QE with a response spectrum consistent with the known atmosphere, fiber and W absorptivity. The bulk of the loss is traceable to known fiber inefficiencies in coupling into the dewar; with improvements to this system, we expect to realize the high intrinsic sensitivity of the W absorber.

## 2. Crab Pulsar Spectrophotometry

On the nights of January 9-11 1999, we observed several sources including the Crab pulsar PSR B0531+21 to illustrate the time and energy capabilities of the device. Despite poor conditions (high cirrus, ∼ 3″ imaging, moon, and suburban light pollution) the data obtained clearly illustrate the potential of this new technology.

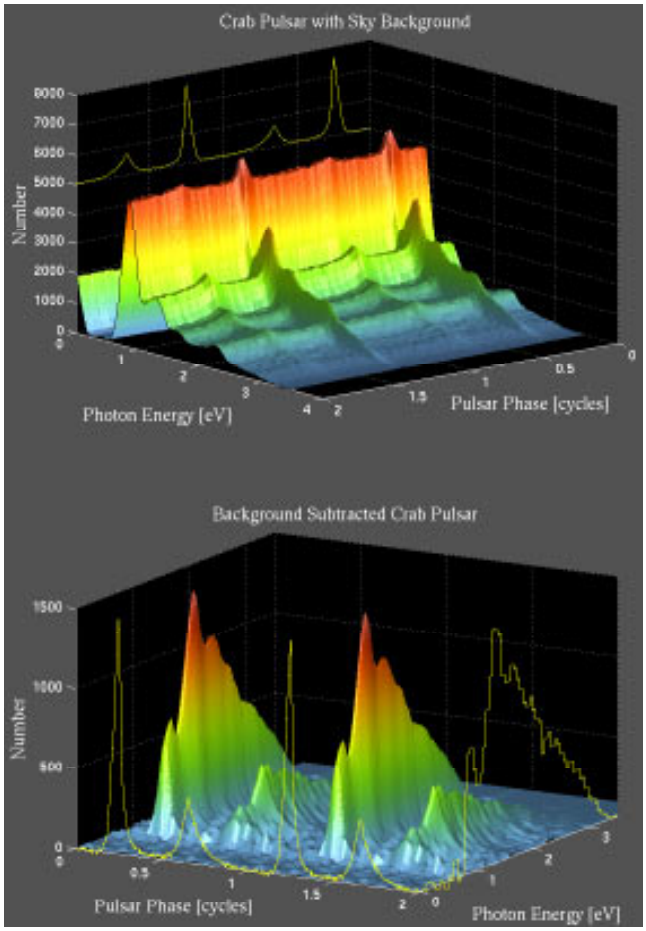


Fig. 2.— Phase resolved spectra of the $P \approx 33.5$ ms Crab pulsar optical/IR emission. Above, the rail-hit corrected count spectra folded into 200 phase bins. Below, after off-pulse sky subtraction.

The photons were barycentered using the current Jodrell Bank radio ephemeris (Lyne, Pritchard and Roberts 1999) and monitored for signal (guiding and atmospheric transmission) and background (cirrus, moon and local lighting) fluctuations. After moderate S/N cuts, some $10^6$ Crab pulsar photons were accumulated into spectra in pulsar phase bins of width 0.005 (168 $\mu$s, Figure 2). Figure 3 shows our folded light curves in visible and near-IR bands. This observation is, to our knowledge, the first simultaneous detection of the Crab at these wavelengths. The curves, normalized at the pulse wings below the half power-point, show a substantial (20%) suppression of the main pulse peak, as noted earlier in lower time-resolution data (Penny 1982). From our light curves,

we find that the shape of the decrement is well fitted by synchrotron self-absorption with an optical depth $\tau \approx 2.7(5.1\times10^4)^{-\alpha}(f_E/30\,\mathrm{mJy})(D_2/l_7)^2(\phi\,B/B_{LC})^{0.5}E_{eV}^{-2.5}$, where the pulsar peak has a power-law flux spectrum $f_E \sim 30E_{ev}^{\alpha}\,\mathrm{mJy}$ with $\alpha$ breaking from $\approx -0.3$ in the UV to $\approx 0$ at 2 eV. This flux is emitted from a region of size $10^7 l_7$ cm near the light cylinder where the field is $B_{LC} \approx 8\times10^5$ G. We assume a distance of $2D_2$ kpc. With these estimates the optical depth fit from our IR band light curve with $\alpha = 0$ gives an $e^{\pm}$ pitch angle $\phi \sim 2\times10^{-3}$. Comparison with flux measurements at longer wavelengths (Middleditch, Pennypacker and Burns 1983) indicates that the phase-averaged spectral break is likely caused by a low energy cut-off in the $e^{\pm}$ spectrum producing a critical frequency $E_c \approx 2$ eV. With our estimated $B$ and $\phi$, the pair spectrum then cuts off at $\Gamma_{e^{\pm}} \approx 400$. Gap models (Romani 1996) predict that different pulse phases arise from regions with varying $B$ and plasma parameters. For example, the second pulse emission stems from lower altitude where a larger dipole $B$ is compensated by a smaller initial $\phi$ and rapid cooling of the $e^{\pm}$ to lower $\Gamma$. Higher S/N data from $0.5-3$ eV following $\alpha$, $E_c$, and $\tau$ through the pulse would allow a map of field and plasma variations through the magnetosphere. We have not detected here IR spectral asymmetries noted (Eikenberry 1997) in the rising and falling slopes of the pulses, but this may be ascribed to our modest IR count statistics. Again higher S/N observations showing these effects would be of interest, as their interpretation is sensitive to the precise IR/optical phasing.

Our flux calibrated spectrum (Figure 4) shows good agreement with published (Middleditch, Pennypacker & Burns 1983) near IR and visible main pulse photometry, although systematic errors in measurement of the calibration stars contribute residuals to the expected synchrotron spectrum exceeding those of count statistics. In addition to measuring spectral variations through the full period (Figure 2), the timing of individual photons allows the search for other periodicities and stochastic fluctuations. For example, 60 Hz line fluctuations are seen in the $\sim 2.1$ eV Na background emission line dominated by street lamps in the San Francisco bay area. We can also examine photon arrival time statistics: our data show that both the counts per period in the main pulse and the distribution of photon arrival times within each pulse are consistent with Poisson at the 95% confidence level, for intervals larger than the maximum 12$\mu$s acquisition system dead time.

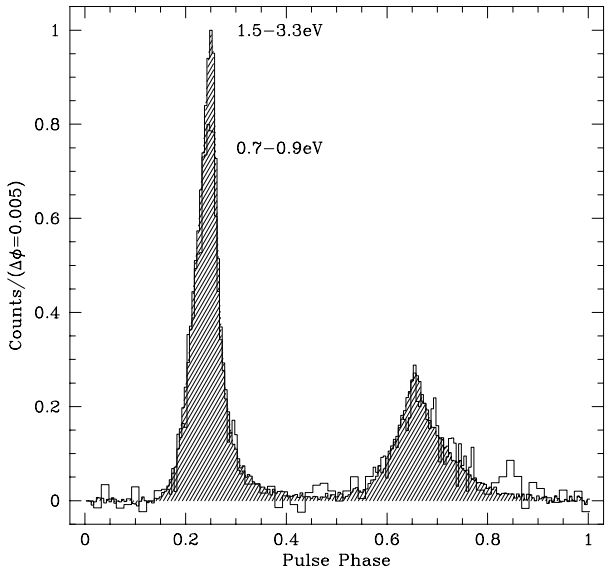


Fig. 3.— Optical and near-IR pulse profiles, showing the $\sim 20\%$ self absorption of the main pulse below 1 eV.

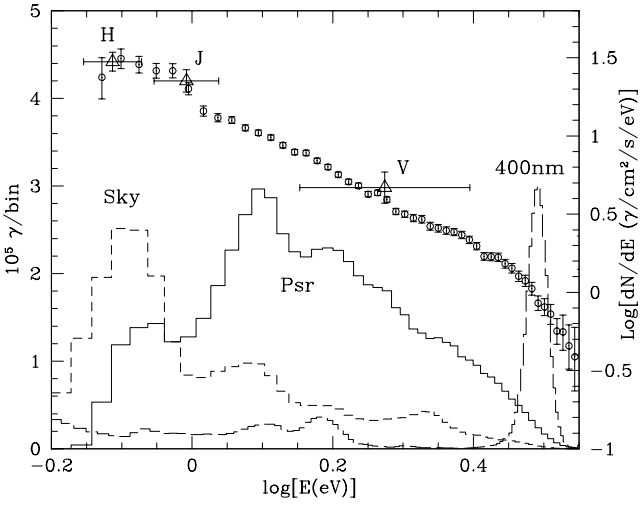


Fig. 4.— Count spectra from a calibration monochromater line (400 nm), along with rail-hit subtracted spectra from the main pulse (Psr, $\phi = 0.215-0.265$) and off-pulse (Sky, $\phi = 0.875-0.125$) intervals. The flux calibrated main pulse (circles) is compared with previously measured (Middleditch, Pennypacker and Burns 1983) main pulse colors (right scale).

## 3. Future Potential

Several improvements to the existing TES sensor have been demonstrated or designed. Count rates up to 30 kHz per read channel have been measured with appropriate tuning of the device transition temperature. Rail masks to eliminate the low energy tail of the PSF can be used to ease IR spectral analysis. Thermal isolation of the W on a $Si_3N_4$ membrane should additionally improve energy resolution to $\sim 0.05$ eV. Multiplexing schemes have been tested (Chervenal, *et al.* 1999) which will allow arrays substantially larger than the few pixel/few read-channel capability of the present system; $\sim$100$\times$100 arrays may be achieved with present multiplexing designs, while advanced schemes are being explored which may allow readout of a programmable subset of megapixel-scale arrays.

Our test data already illustrate the potential of a TES spectrophotometer for studies of pulsars and stochastically fluctuating (*e.g.*, interacting black hole and neutron star binary) compact object sources. Important experiments probing emission zone structures, pulsar plasma

physics and relativistic photon propagation follow immediately from observations with the existing system at large aperture telescopes. Even modest scale arrays should enable further applications in many fields. For example in biochemical studies time- and energy-resolved fluorescence imaging of multiply labeled biomolecules can characterize configuration and chemical activity on $\mu$s timescales. A number of important applications for astrophysics and cosmology have also been noted (Jakobsen 1999) for such detectors. The most striking progress will, of course, stem from placement of a TES array system in space, where diffraction-limited pixels and cool optics allow *simultaneous* observation over some two decades of photon energy. To illustrate, Figure 5 shows simulated count spectra with a small (1 m) aperture and modest exposure. The modeled sources are comparable to the *faintest* galaxies and galaxy components detected in the Hubble Deep Field (Williams, *et al.* 1996). TES areal spectrophotometry should enable a whole new class of studies, providing morphology, redshift, spectral classification, and chemical evolution studies at the present limits of visibility in the universe.

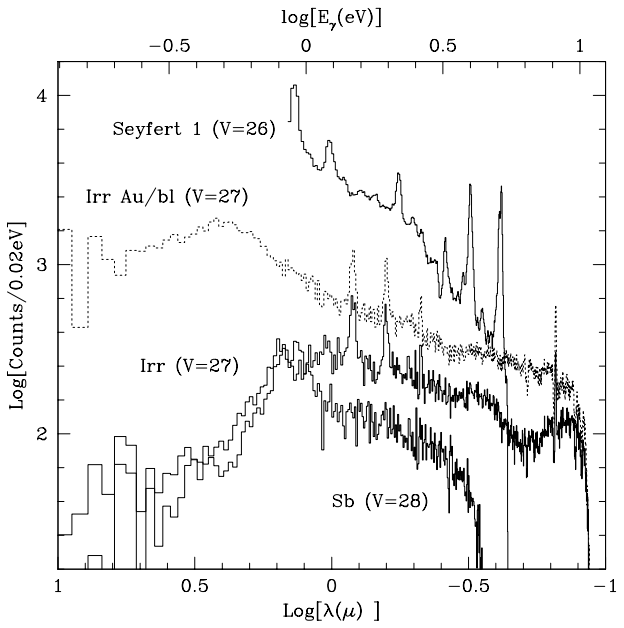


Fig. 5.— Simulated background subtracted spectra from one 0.1″ pixel of a TES array on a 1 m aperture space telescope. Passively cooled optics, zodiacal background from moderate ecliptic latitude, 0.05 eV resolution and 10 h exposure are assumed. Sample synthetic spectra (Fioc & Rocca-Volmerange 1997) show a portion of an Sb galaxy ($M = 10^9 M_\odot$, $z = 2$) a low mass irregular galaxy ($M = 1.5 \times 10^9 M_\odot$, age=30My, $z = 0.25$) and a low luminosity Seyfert 1 nucleus (scaled from NGC5548 (STScI AGN atlas); $m_V = 26$, $z = 1$). The dashed line shows the increased S/N expected from coating the bare W with an absorbing (*e.g.*, Au-black) film. Continuum breaks and a number of lines are well detected; broad (*e.g.*, AGN) lines are resolved in the blue.

This work was supported in part by grants from NASA (NAG5-3775 and NAG 5-3263), from the DOE (DE-FG03-90ER40569) and from the Research Corporation; devices were fabricated in the Stanford Nanofabrication facility. We thank Kent Irwin and John Martinis of NIST for continued collaboration on TES and SQUID technology.

## REFERENCES

Cabrera, B., *et al.* 1998, *Appl. Phys. Let.*, **73**, 735.
Chervenal, J.A., *et al.* 1999, *Appl. Phys. Lett.*, submitted.
Eikenberry, S.S., *et al.* 1997, *ApJ*, **476**, 281.
Fioc, M. & Rocca-Volmerange, B. 1997, *AA*, **326**, 950.
Gunn, J.E. & Stryker 1983, L.L., *ApJ Suppl.*, **52**, 121.
Harris, L. 1956, *J. of Op. Soc. Am.*, **46**, 160.
Humbach, O., *et al.* 1996, *J. of Non-Cryst. Sol.*, **203**, 19.
Irwin, K.D. 1995, *Appl. Phys. Lett.*, **66**, 1998.
Jakobsen, P. 1999, in Ultraviolet-Optical Space Astronomy Beyond HST, eds J. A. Morse, J. M. Shull, & A. L. Kinney, ASP Conf. Ser., in press
Lyne, A.G., Pritchard, R.S. and Roberts, M.E. 1999, (http://www.jb.man.ac.uk/ pulsar/crab.html)
Middleditch, J., Pennypacker, C. & Burns, M.S. 1983, *ApJ*, **273**, 261.
Peacock, A. et al. 1996, *Nature*, 381, 135
Penny, A.J. 1982, *MNRaS*, **198**, 773
Perryman, M.A.C., Favata, F., Peacock, A., Rando, N. and Taylor, B.G. 1999, *AA*, in press.
Romani, R.W. 1996, *ApJ*, **470**, 469.
Romani, R.W., *et al.* 1998, *BAAS*, **30**, 1266.
Welty, R. & Martinis, J. 1993, IEEE Trans., Appl. Supercond. **3**, 2605.
Williams, R.E., *et al.*, 1996, *AJ*, **112**, 1335

This 2-column preprint was prepared with the AAS LaTeX macros v4.0.